


Borderline Magnetism: How Adding Mg to Paramagnetic CeCo₃ Makes a 450-K Ferromagnet with Large Magnetic Anisotropy

Tribhuwan Pandey* and David S. Parker†

Material Science and Technology Division, Oak Ridge National Laboratory, Oak Ridge, 37831 Tennessee, USA

 (Received 19 February 2018; revised manuscript received 9 July 2018; published 19 September 2018)

A recent experimental study [Phys. Rev. Appl. 9, 024023 (2018)] on paramagnetic CeCo₃ finds that magnesium alloying induces a ferromagnetic transition with intrinsic properties large enough for permanent magnet applications. Here we explain these surprising results via a first-principles study of the electronic structure and magnetism of magnesium-alloyed CeCo₃. We find the origin of this magnesium-induced ferromagnetic transition to be Stoner physics—the substantial increase in the Fermi-level density of states $N(E_F)$ with Mg alloying. Our calculations suggest that both Ce and Co atoms are likely to be important for generating large magnetic anisotropy suggesting the viability of Co-3*d* and Ce-4*f* interaction for the generation of magnetic anisotropy in magnetic materials. These results offer a route to the discovery of ferromagnetic materials and provide fundamental insight into the magnetic properties of these alloys.

DOI: [10.1103/PhysRevApplied.10.034038](https://doi.org/10.1103/PhysRevApplied.10.034038)

I. INTRODUCTION

Magnetism and magnetic materials have been known colloquially since antiquity, with lodestone's magnetic properties, such as its attraction to iron, noted in ancient texts [1,2]. More recently, with the industrial, scientific, and technological revolutions occurring since the latter half of the 19th century has come increasing interest in *explaining* magnetic behavior. This has often been related to the properties of exchange: the process by which the Pauli exclusion principle, combined with local crystal structure, results in the moments of magnetic ions such as iron or manganese aligning parallel, or antiparallel, to their nearest-neighbor magnetic ions. Noncollinear states and more complex ordering patterns are also frequently observed with neutron scattering [3–7].

Density-functional theory (DFT), as originally formulated by Kohn and Sham [8–11] and implemented by Perdew [12–14] and others [15,16], has become a useful tool for the study of such systems, leading to the ability to understand and even *predict* the behavior of magnetic materials. This has led to increasing interest in “high-throughput” calculations [17–20], in which a large number of materials are rapidly screened via DFT in an attempt to find properties technologically useful for applications such as permanent magnets. In general, these calculations usually predict the proper (or occurrence of a) magnetic ground state and often attain good agreement (i.e., within 10%) with experimentally measured magnetic moment

values, while calculations of magnetic anisotropy are more difficult, particularly for rare-earth compounds such as the permanent magnet workhorse Nd₂Fe₁₄B [21–24].

Recently, Canfield *et al.* [25] found ferromagnetic behavior in the cerium-cobalt intermetallic CeCo₃ upon alloying with Mg. Perhaps surprisingly, despite containing 75 at. % of the ferromagnetic Co, which orders at 1388 K [26,27], CeCo₃ does not order magnetically. However, alloying of this compound with Mg not only renders it ferromagnetic, but does so with a Curie point T_C as high as 450 K and a large 50-K magnetic anisotropy of 2.2 MJ/m³. These Curie point and anisotropy values are in the range of potential permanent magnets, although this specific material would likely require substantial further optimization for actual usage as a permanent magnet. How does adding a nonmagnetic element to paramagnetic CeCo₃ yield a 450-K ferromagnet with large magnetic anisotropy?

Here, we answer this basic question. We find its resolution in Stoner physics—the substantial increase in the Fermi-level density-of-states $N(E_F)$ with Mg alloying—and in the magnetic anisotropy of the Ce-4*f* and Co-3*d* orbitals. This study is organized as follows. First, we describe the calculation methods, the essential input parameters, and the approximations adopted to achieve the desired numerical convergence. Next, we discuss the calculated properties of the base compound CeCo₃, finding that the properties of CeCo₃ are sensitive to the exchange-correlation potential [local-spin-density approximation (LDA) or generalized-gradient approximation (GGA)]. We then describe the magnetic properties of the Mg-substituted compound (Ce₂Co₉Mg). We show that the experimentally observed enhancement in magnetic

*pandeyt@ornl.gov

†parkerds@ornl.gov

properties is described by the Stoner picture. The experimental results on the Mg-substituted alloys are fully corroborated by our first-principles calculations. Finally, we show that these and related results [28] on Mg-alloyed NdCo₃ and other ferromagnets open a pathway for the development of high-performance magnets.

II. THEORETICAL METHODS

The calculations are performed by using the all-electron-density functional code WIEN2K [29] at the experimental lattice parameters [25], which are listed in Table I. The internal coordinates are relaxed until forces on all the atoms are less than 1 mRy/bohr. Muffin-tin sphere radii of 2.5 for Ce, 2.2 for Co, and 2.1 for Mg are used. For good basis-set convergence, a RK_{max} value of 7.0 is used. RK_{max} denotes the product of the largest plane-wave expansion wave vector and the smallest muffin-tin radius. The magnetic-anisotropy energy (MAE) is obtained by calculating the total energies of the system with spin-orbit coupling (SOC) as $K_1 = E_a - E_c$, where E_a and E_c are the total energies for the magnetization oriented along the in-plane [110] and out-of-plane [111] directions. For the structure relaxation, 1000 **k** points are used in the full Brillouin zone. MAE as a small quantity (of the order of meV) can sensitively depend on the number of **k** points used. The difference in MAE calculated using 6000 and 4000 **k** points is less than 4% and all the MAE results reported here use 4000 **k** points. The convergence of MAE with respect

TABLE I. The experimental lattice constants from Ref. [25] employed in our calculations along with the calculated spin (within the sphere [44]) ($\mu_{\text{Co/Ce}}^{\text{spin}}$), orbital magnetic moments ($\mu_{\text{Co/Ce}}^{\text{orb}}$), and magnetic anisotropy (K_1). The experimentally measured magnetic moments ($m_{\text{tot}}^{\text{exp}}$) and magnetic anisotropy [K_1 (exp.)] are also shown for comparison. The calculations for CeCo₃ are done within LDA, and calculations for Ce₂Co₉Mg are done within LDA+SOC+ U ($U_{\text{Ce}} = 1.5$ eV). K_1^{OC} denotes the MAE value calculated within an open-core approximation, where Ce-4*f* electrons are treated as core electrons.

Compound	CeCo ₃	Ce ₂ Co ₉ Mg
a (Å)	4.94	4.92
c (Å)	24.64	24.01
c/a	4.98	4.87
Volume (Å ³)	521.33	504.75
$\mu_{\text{Co}}^{\text{spin}}$ (μ_B)	0.33	1.17
$\mu_{\text{Co}}^{\text{orb}}$ (μ_B)		0.09
$\mu_{\text{Ce}}^{\text{spin}}$ (μ_B)	-0.20	-0.51
$\mu_{\text{Ce}}^{\text{orb}}$ (μ_B)		0.23
m_{tot} (μ_B /per f.u.)	0.71	10.04
$m_{\text{tot}}^{\text{exp}}$ (μ_B /per f.u.)	$0 \lesssim 0.40$ [25,42]	8.0 [25]
K_1 (MJ/m ³)		2.10
K_1^{OC} (MJ/m ³)		0.22
K_1 (exp.) (MJ/m ³)		2.20 [25]

to **k** points is discussed in the Appendix. The accurate calculation of MAE for rare-earth-transition-metal complexes within the conventional LDA/GGA framework is challenging. Within these DFT approaches, the partially filled rare-earth *f* states are pinned at the Fermi level, which results in incorrect properties. This problem can be remedied by treating the *f* electrons as unhybridized core states (the open core approximation [30]). However, this approximation often results in the wrong value of the MAE [31,32]. Another approach is to consider *f* electrons as valence electrons and introduce a Hubbard U correction to the *f* orbitals, which splits the *f* bands into lower and upper Hubbard bands. This is known as the LDA+ U approach and we follow this approach here. Here, LDA+ U corrections are included for the Ce-4*f* orbitals using the self-interaction correction (SIC) [33–36] for the double-counting correction. In all the calculations, Hund’s coupling parameter J is set to 0 eV. As the Co states in Ce₂Co₉Mg are not localized, a U correction is not used for Co sites. As discussed in the following sections, introducing a U for Ce-*f* orbitals is crucial in the prediction of the correct magnetic anisotropy and orbital magnetic moments. We find that MAE calculated with $U = 1.5$ eV is in good agreement with experiments.

III. RESULTS AND DISCUSSION

A. Properties of CeCo₃

The unit cell and primitive cell (used in our simulations) are shown in Figs. 1(a) and 1(b). CeCo₃ crystallizes in a rhombohedral structure with space group $R\bar{3}m$. In this structure Co atom has three independent sites, namely, 3*b*, 6*c*, and 18*h*, whereas Ce atom has two independent sites (3*a* and 6*c*). As shown in Fig. 1, both Ce sites have different arrangement of nearest neighbors. While the Ce-3*a* site is surrounded by six Co-6*c* (first-nearest) and 12 Co-18*h* (second-nearest) neighbors, the Ce-6*c* site has six first-nearest (Co-18*h*) and only three (Co-3*b*) second-nearest neighbors. Numerous prior studies [37–41] on the weak itinerant magnetic systems have shown that the choice of functional can be very important in predicting the correct magnetic ground state. Hence, first a comparative analysis of the LDA and GGA functional for CeCo₃ is performed. These results are discussed in the Appendix (Fig. 7). While both LDA and GGA calculations favor a ferromagnetic state, at experimental lattice parameters within LDA, the energy difference between the ferromagnetic and nonmagnetic state ($E_{\text{FM}} - E_{\text{NM}}$) is only -1.9 meV on a per-Co basis. On the other hand, within GGA, this difference is about -21 meV per Co atom. This result is consistent with the well-known tendency of the GGA to exhibit stronger magnetic instabilities than the LDA. Also, the Co magnetic moment calculated at experimental lattice parameters within LDA ($0.33 \mu_B$) and GGA ($0.99 \mu_B$) functionals

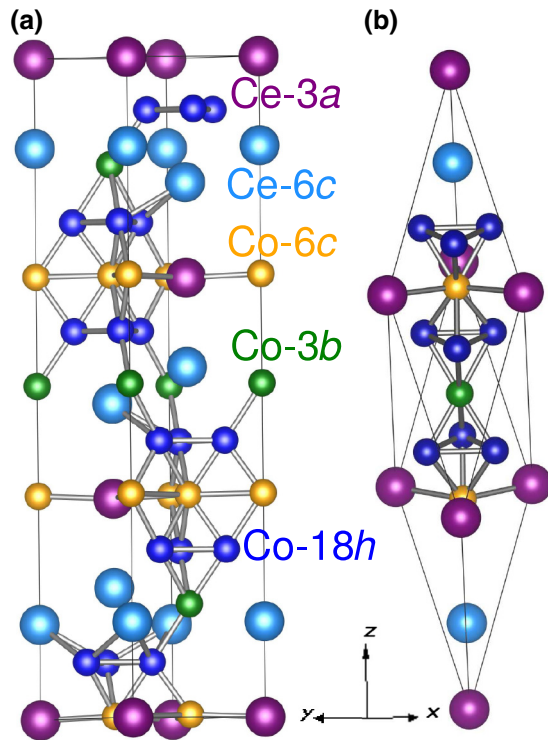


FIG. 1. Schematic representation of the crystal structures of CeCo_3 . Nonequivalent Ce atoms are shown in magenta (Ce-3a) and cyan color (Ce-6c). The nonequivalent Co-3b, -6c, and -18h sites are shown by orange, green, and blue spheres, respectively. (b) The primitive cell used for calculating the properties.

is very different. Experimentally, CeCo_3 is often characterized as a Pauli paramagnetic [25,42], although there is older literature [43] that has found evidence for a magnetic character in CeCo_3 . This research suggests that CeCo_3 is at or near a magnetic instability, which is better represented in this case by the LDA approach, with its much smaller magnetic energy (-1.9 meV/Co). Unless otherwise stated, all the calculations presented in the following sections are, therefore, performed using the LDA at the experimental lattice constants from Ref. [25].

B. Effect of Mg substitution on magnetic properties of CeCo_3

As mentioned previously, the primary question that theory should answer is how Mg alloying transforms the Pauli paramagnet CeCo_3 into a ferromagnet with properties (T_c of 450 K and a low-temperature anisotropy field of 10 T) comparable to those of known permanent magnets. The basic reason for this behavior can, in fact, be seen from Fig. 2. There, we plot the calculated nonmagnetic density of states (DOS) of the base compound CeCo_3 , calculated within the LDA approximation. For simplicity, in this calculation, we omit the spin-orbit coupling and the Hubbard U , which will play an important role in detailed comparison with experiment later.

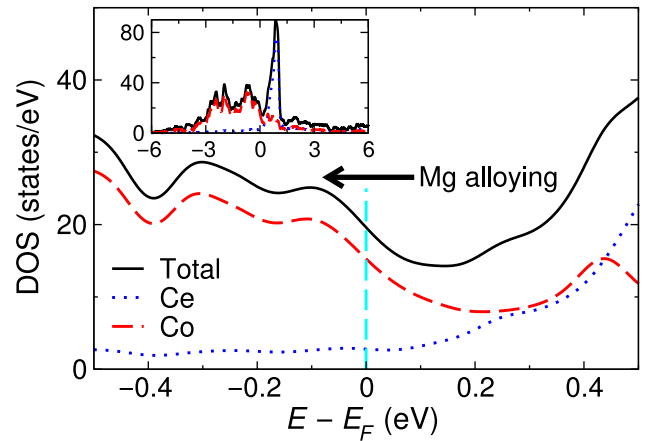


FIG. 2. The calculated nonmagnetic density of states of CeCo_3 with LDA functional. For simplicity, neither the spin-orbit coupling nor a Hubbard U is included. Note the rapid increase in both total and Co DOS as the energy is reduced below E_F (vertical cyan line), which occurs with alloying of Mg. DOS over a wide energy window is shown in the inset.

The plot depicts the calculated DOS in a narrow window around the Fermi level (E_F) (main plot) and for several eV around E_F in the inset. From the inset, we see two main features: the large Ce peak (in blue), from the unoccupied localized $4f$ states, centered around 1 eV above E_F , and the Co DOS, mainly from -4 eV to $+1$ eV (in red). The Co DOS provides the majority of the spectral weight around E_F , suggesting the Co as being the “driving force” for magnetism in the $\text{Ce}_{3-x}\text{Mg}_x\text{Co}_9$ alloy system. In the main plot, we see that for energies below the E_F , the DOS increases rapidly, both for the total and for the Co. Indeed, at an energy 0.18 eV below E_F , the values for these quantities are nearly 1.5 times higher than the Fermi-level values of 19.0 and 15.3 per eV-unit cell (note that the primitive cell contains nine Co, or three formula units). This result immediately suggests that “hole doping” (borrowing a term from semiconductor physics) tends to increase the Fermi-level DOS. Now, the Stoner criterion [45] states that a ferromagnetic instability occurs when the condition $IN(E_F) > 1$ is fulfilled. Here, I is the Stoner parameter, which we compute by calculating the average exchange splitting (ΔE_{ex}) and by using the relation $\Delta E_{\text{ex}} = Im_{\text{avg}}$ [46]. Here, m_{avg} is the average magnetic moment of the Co atom in CeCo_3 . We find I as 0.56 eV, which is quite close to 0.49 eV value for elemental Co [47]. Additional details involving the calculation of I are listed in the Appendix. For our purposes, $N(E_F)$ should be understood as the total Co DOS, on a per-Co basis. Hence, hole doping should be understood as likely to render CeCo_3 more magnetic.

Our calculations find the valency of Ce in CeCo_3 to be dependent on the approximation used (see Fig. 8 and the corresponding discussion in the Appendix). This dependence of Ce valency implies possible valence fluctuations

in CeCo_3 , a detailed study of which is beyond the scope of this work. Such valence fluctuations do occur in rare-earth compounds [48–55]. In our conventional LDA (without SOC and without U) calculations, Ce in CeCo_3 is tetravalent, which is consistent with the experimentally observed nonmagnetic behavior, while Mg is nearly universally in a +2-charge state. Therefore, Mg donates two fewer electrons to the bands than Ce and thus tends to result in effective “hole doping,” an increase in Fermi-level DOS, and thereby an increase in ferromagnetic behavior, consistent with experiment. For CeCo_3 , the total Co non-spin-polarized $N(E_F)$ is 15.7 states/eV-unit cell or 1.7 states/eV on a per-Co-atom basis, indicating that the Stoner criterion (taking I as approximately 0.56 eV, as described in the Appendix) is very nearly satisfied [$IN(E_F) \sim 0.98$]. On the other hand, at 0.18 eV below the Fermi level, the Stoner criterion [$IN(E_F) \sim 1.47$] is clearly fulfilled.

The previous analysis is done within a “rigid-band” picture, in which the primary effect of Mg alloying is a reduction in the Fermi energy. However, one should not thereby argue that correlations are unimportant in this system—we will see that they are indeed important in generating magnetic anisotropy. The correlations here generally apply to the Ce atom, not to the Co atom. As in many rare-earth magnets, it is the $3d$ (in this case Co) atoms that are generally driving the magnetic *instability*.

C. Magnetic properties of $\text{Ce}_2\text{Co}_9\text{Mg}$

As discussed in the previous section based on electronic structure and Stoner theory analysis, the observed ferromagnetism in CeCo_3 upon Mg substitution can be explained based on Stoner physics. Next, we calculate the magnetic properties of $\text{Ce}_2\text{Co}_9\text{Mg}$. We begin with identifying the proper ground state structure for $\text{Ce}_2\text{Co}_9\text{Mg}$. The recent experimental efforts [25] conclude that Mg alloying in CeCo_3 prefers to occupy the Ce-6c site and the structure maintains its rhombohedral symmetry. To mimic such a structure, Mg atoms are substituted in 50-50 fashion among six available Ce-6c sites in the 36-atom unit cell. These configurations are presented in Fig. 3(a). All three structures are relaxed to their ground state by minimizing the total forces. While for configuration 1 and configuration 2 the rhombohedral symmetry is broken and the structures transform into a less symmetry-trigonal cell (with space group $P3m1$), configuration 3 maintains its rhombohedral symmetry (space group $R-3m$). Energetically, we find configuration 3 to be most stable, whereas configurations 1 and 2 are higher in energy (unstable) by only 8.3 meV relative to configuration 3. To make sure that the calculated magnetic properties are independent of the configuration used, we next compare their DOS near the Fermi level, which is shown in Fig. 3(b). We find that the DOS of all three configurations are nearly

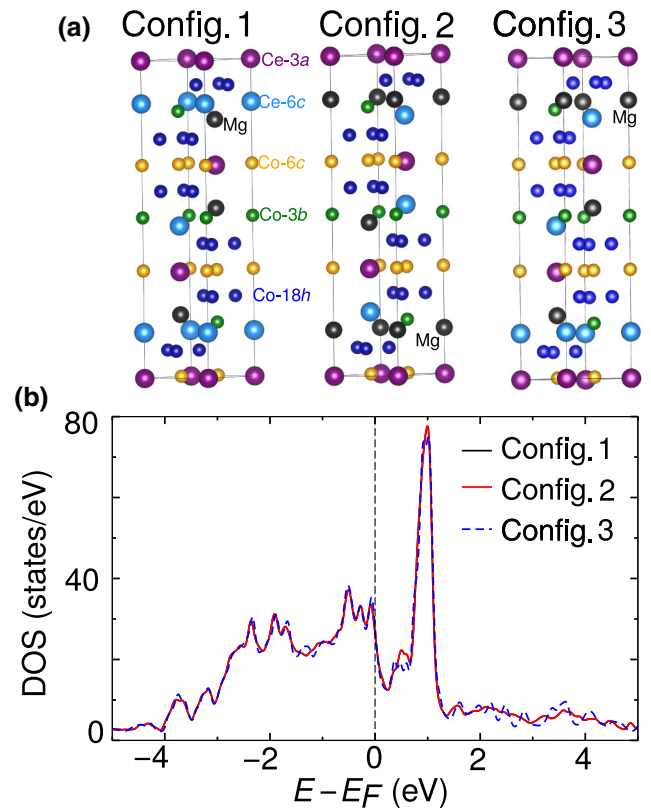


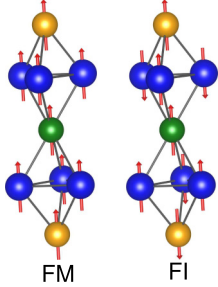
FIG. 3. (a) The configurations used for substituting Mg (shown by black spheres) in a CeCo_3 unit cell. (b) The non-spin-polarized density of states calculated within LDA.

identical. As the magnetic properties and MAE are dependent on the behavior of the DOS in the vicinity of the Fermi level, the nearly similar DOS implies that the calculated magnetic properties should be independent of the configuration used. Also, as the experimental study finds the structure to be rhombohedral, configuration 3 is used in all the calculations for $\text{Ce}_2\text{Co}_9\text{Mg}$.

In order to predict the accurate magnetic ground state of $\text{Ce}_2\text{Co}_9\text{Mg}$, various collinear spin configurations with different spin arrangements of Co atoms are considered. Nearly all of the configurations (with the exception of the ferrimagnetic state shown in Table II) converged to the stable ferromagnetic state. As observed in the experimental measurements, we find a ferromagnetic behavior in $\text{Ce}_2\text{Co}_9\text{Mg}$, with a calculated average magnetic moment of $1.18 \mu_B$ per Co, as shown in Table I. This includes an average orbital magnetic moment of approximately $0.09 \mu_B$ on the Co site. As can be seen from Table I, compared to the base compound CeCo_3 , upon Mg alloying ($\text{Ce}_2\text{Co}_9\text{Mg}$), the magnetic moment on the Co site is enhanced by more than 3.5 times. Because of different site symmetry, the Ce sites have different orbital magnetic moments of $0.20 \mu_B$ for Ce-3a and $0.16 \mu_B$ for the Ce-6c sites. Upon introducing a Hubbard U , the Ce orbital magnetic moment

TABLE II. The calculated energy difference (ΔE) between the FI state and FM state on a per-Co-atom basis. The calculated mean-field Curie temperatures ($\Delta E/3$) are also shown. The inset on the left is a schematic defining the ferrimagnetic (FI) and ferromagnetic (FM) configurations of Co atoms in the $\text{Ce}_2\text{Co}_9\text{Mg}$ primitive cell used in Curie point calculations. Sphere colors correspond to the same Co sites as in Fig. 1.

System	ΔE (meV/Co)	T_C (K)
CeCo_3	1.9	7
Ce_2MgCo_9	54.8	212
CeMg_2Co_9	87.8	339



increases and, for $U = 1.5$, it becomes $0.27 \mu_B$ for Ce-3a and $0.19 \mu_B$ for the Ce-6c sites. The U dependence of the Ce orbital magnetic moment is discussed in the next section. As expected, Ce atoms prefer to be antialigned with respect to Co with an average magnetic moment (including an average orbital magnetic moment of $0.23 \mu_B$) of $-0.28 \mu_B$ per Ce atom. This result is similar to numerous other rare-earth magnet results [56,57]. The calculated total magnetic moment of $10.04 \mu_B$ per formula unit is in fair agreement with the 50-K experimental value of about $8.0 \mu_B$. For $\text{Ce}_{1.67}\text{Mg}_{1.33}\text{Co}_9$, this deviation in the predicted magnetic moment can be explained with the decreasing trend of the saturation moment of $\text{Ce}_{3-x}\text{Mg}_x\text{Co}_9$ samples higher than $x = 1.11$, as discussed in Ref. [25]. We present the DOS in Fig. 4. The magnetic moments on Co sites are somewhat lower than that observed in SmCo_5 and YCo_5 [58,59] ($1.51 \mu_B$ per Co). This result is also corroborated by the DOS plot where the spin-up DOS is substantially lower than the spin-down DOS around E_F , reducing the magnetic moment. The enhanced ($\times 15$) Mg DOS is also shown in Fig. 4(b). Although the contribution of the Mg DOS at Fermi level is small, there is some hybridization present with the neighboring Co and Ce atoms, particularly in the majority-spin channel. The Mg-s states hybridize strongly with neighboring Co atoms at around -4 eV below the Fermi level. Both Ce sites have large DOS above the Fermi level. The enlarged Ce DOS in the vicinity of the Fermi level is shown in the inset of Fig. 4. In the minority-spin channel, the Ce-3a site has relatively larger DOS, which is consistent with the higher calculated magnetic moment. As explained before, alloying with Mg results in the enhancement of the Co DOS in the vicinity of the Fermi level, improving the magnetic properties as well as the Co moments.

We examine the spin and orbital character of the orbitals near the Fermi level [60–63]. It is well known that the magnetocrystalline anisotropy arises under the influence

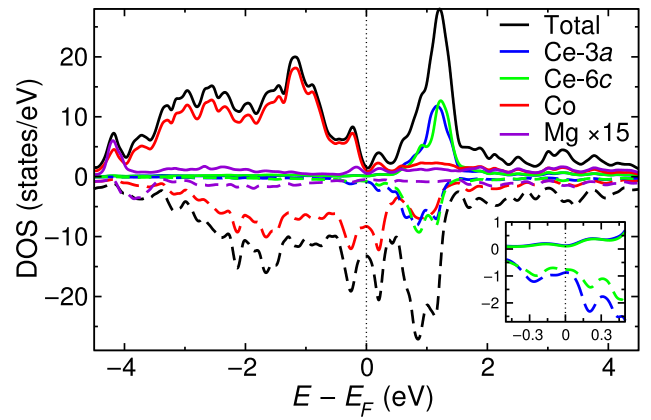


FIG. 4. The calculated density of states of Ce_2MgCo_9 . The solid and dotted lines denote the density of states for spin-up and spin-down channels, respectively. The Mg DOS is enlarged by 15 times for clarity. The Co DOS is averaged over all nine Co atoms. The inset shows the enlarged Ce DOS near the Fermi level. The DOS is computed within LDA+SOC+ U with $U = 1.5$ eV at the Ce site.

of spin-orbit coupling and may be expressed as a second-order perturbative interaction between occupied and unoccupied states. The scalar-relativistic partial densities of states (PDOS) projected on the various nonequivalent Co sites are shown in Fig. 5. Without SOC, five Co- d orbitals split into three groups $m = 0$ (d_z^2), $m = \pm 1$ ($d_{yz}|d_{xz}$), and $m = \pm 2$ ($d_{x^2-y^2}|d_{xy}$) and they are shown in Fig. 5 with red, blue, and black (gray filled) lines, respectively. In this plot, we use the LDA without a spin orbit coupling or a Ce U . Notably, all the d orbitals hybridize with the neighboring atoms and, overall, the DOS exhibits broad bandwidth (atomiclike narrower bands are not present). As expected, all three nonequivalent Co sites have large DOS in the majority-spin channel just below the Fermi level, but very small DOS at the Fermi level itself. In particular, for Co-3b and Co-6c sites, the contribution from $d_{xz}|d_{yz}$ orbitals ($m = \pm 1$) dominates, while for Co-18h, a significant contribution from $d_{x^2-y^2}|d_{xy}$ orbitals is also present. The minority-spin channel shows significant DOS at and around the Fermi level for all three Co sites. The highest contribution from $d_{x^2-y^2}|d_{xy}$ along with d_{z^2} for Co-3b, from $d_{x^2-y^2}|d_{xy}$ and $d_{xz}|d_{yz}$ for Co-6c, and from $d_{xz}|d_{yz}$ and $d_{x^2-y^2}|d_{xy}$ for Co-18h can be seen. Overall, a complex behavior is observed, making a quantitative analysis of the origin of the MAE difficult. As described later, this difficulty is compounded by the substantial dependence of the calculated MAE on the value of U assumed for Ce. What we can say is that multiple Co orbitals contribute to the magnetic behavior, likely including the MAE, in a manner specific to each distinct site, with the magnetic properties of the Co atoms substantially impacted by a large spin-down DOS near E_F .

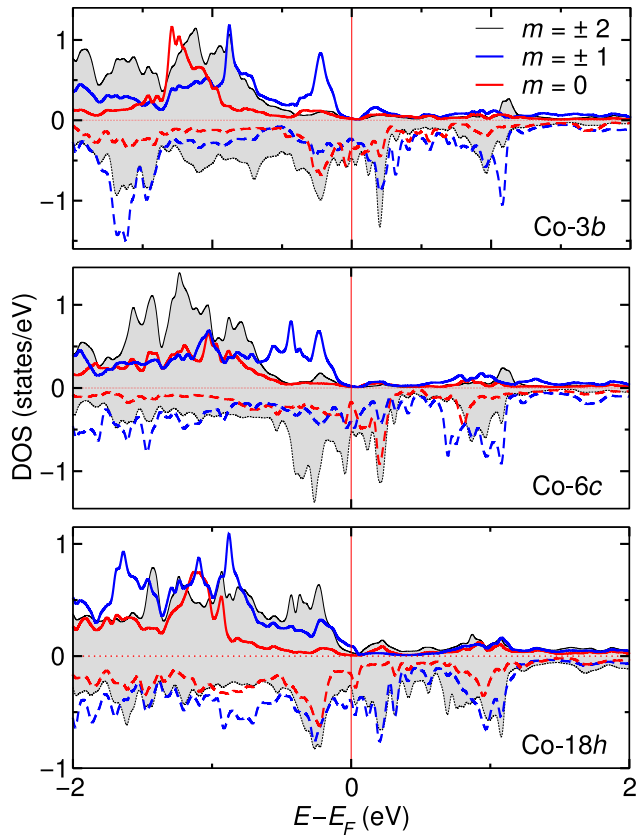


FIG. 5. The spin-polarized partial density of states projected on the $3d$ states of nonequivalent Co sites in $\text{Ce}_2\text{Co}_9\text{Mg}$. The black (gray filled), blue, and red colors indicate the contribution from $m = 2$ (degenerate d_{xy} and $d_{x^2-y^2}$ states), $m = 1$ (degenerate d_{xz} and d_{yz}), and $m = 0$ (d_{z^2}) states, respectively. Positive and negative DOS represent majority- and minority-spin channels, respectively. These calculations are done within LDA, without spin-orbit coupling and without U .

D. Magnetic anisotropy energy for $\text{Ce}_2\text{Co}_9\text{Mg}$

Next, we calculate the MAE for $\text{Ce}_2\text{Co}_9\text{Mg}$, which is tabulated in Table I. First, a calculation without including a Hubbard U parameter is performed. The MAE calculated without including the U at the Ce site is about 0.46 MJ/m^3 , much smaller than the experimental K_1 value of 2.2 MJ/m^3 . This result suggests that, to improve the agreement between theory and experiments, a correlated approach is necessary. The dependence of the MAE on the U parameter is shown in Fig. 6(a). We find from LDA+ U +SOC calculations that the MAE is sensitive to the U parameter used and increases to 2.10 MJ/m^3 (2.25 meV/f.u.) at $U = 1.5 \text{ eV}$. This result is in good agreement with the experimental value of 2.2 MJ/m^3 . This U value is somewhat smaller than that typically taken for Ce and, for more typically employed values of U (3 or 4 eV), one finds very different values of the MAE, with the MAE even becoming negative for U past 3.5 eV. The strong dependence of MAE on U argues for the relevance

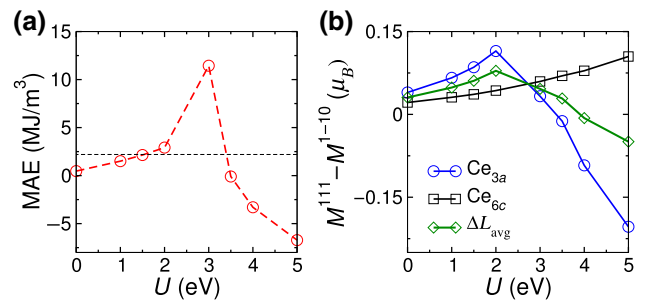


FIG. 6. (a) Dependence of the MAE with respect to the U parameter at the Ce site. The circles denote the calculated data points. Note that the line is a guide to the eye. The experimental value of the MAE [25] is shown with a dashed black line. (b) Variation of orbital magnetic moment anisotropy (ΔL) at the Ce-3a and Ce-6c sites as a function of U at the Ce site. Variation in average orbital moments (ΔL_{avg}) is shown by diamonds. These calculations are done within LDA+SOC+ U .

of correlations in treating Ce here and for the importance of Ce in generating magnetic anisotropy. To further show the importance of Ce- $4f$ states for generating the MAE, we also calculated the MAE by treating Ce- f states as core electrons (known as open-core approximation). As shown in Table I, the MAE calculated within open-core approximation is very small (0.22 MJ/m^3), implying that Ce- f valence electrons play an important role in the magnetic properties of $\text{Ce}_2\text{Co}_9\text{Mg}$. The MAE can also be correlated to the anisotropy of orbital magnetic moment by following the Bruno relation [64] $\text{MAE} = \sum_j \lambda_j \Delta L_j \cdot S_j$. Here, λ_j , ΔL_j , and S_j refer to the spin-orbital coupling constant, anisotropy of orbital magnetic moment, and spin moment of atomic species j , respectively.

The dependence of orbital magnetic moment anisotropy (ΔL) on the U value for nonequivalent Ce sites is shown in Fig. 6(b). ΔL is computed by taking the difference between orbital magnetic moment along the out-of-plane [111] direction and the in-plane [110] direction. We find that the Ce-3a and Ce-6c sites exhibit very different orbital-moment dependence on U . At $U = 0$, both sites have nearly the same ΔL . While for a U value in between 0 and 2 eV, the Ce-3a site exhibits a higher orbital magnetic moment along the out-of-plane direction and ΔL is positive, it becomes negative as U becomes larger than 2 eV. The situation is rather different for the Ce-6c site, and for all the U values investigated here, ΔL remains positive and exhibits a relatively much weaker dependence on U . This different orbital magnetic moment for different Ce sites suggest that the role of Ce in generating the MAE for this compound is rather complex and site specific. The U dependence of average Ce ΔL_{avg} is also shown in Fig. 6(b). Because of its large ΔL , the trend of ΔL_{avg} is governed by the Ce-3a site. For the most part, the MAE follows the Bruno relation and can be (qualitatively) explained by the trend of ΔL , with the only exception to this at $U = 3 \text{ eV}$.

While the strength of SOC for $4f$ rare-earth electrons is approximately 0.5 eV, for $3d$ transition metals, it is an order of magnitude or more smaller. This result, together with our calculated $\Delta L_{Ce} = 0.060 \mu_B$ (at $U = 1.5$ eV) and $\Delta L_{Co} = 0.009 \mu_B$, indicates that the majority of the MAE should originate from Ce atoms. Usually, the individual atomic contribution to the MAE can also be quantified by selectively switching off the SOC on the different atomic sites. However, for Ce_2Co_9Mg , such an analysis does not give consistent results and the total MAE calculated by adding the contribution from individual atomic sites is 60% larger than the actual MAE (obtained by applying the SOC at both the Ce and Co sites simultaneously). This difference suggests that analyzing the atomic origin of the MAE in this compound is far more complicated and considering cross Ce-Co spin-orbit coupling terms may be essential. Nonetheless, while given their great spectral weight near E_F in Fig. 2 it is the Co atoms that drive the magnetic instability, both Co and Ce atoms are important for the MAE.

E. Effect of Mg alloying on the Curie point

Perhaps the most remarkable observation of the recent experimental measurements [25] is the considerable increase in Curie temperature of $CeCo_3$ by alloying with Mg. Generally, for a local-moment ferromagnetic system, the Curie temperature may be estimated by the energy difference ($\Delta E = E_{AF} - E_{FM}$) between an antiferromagnetic structure (AF), where the nearest neighbors of all Co atoms are antialigned, and the ferromagnetic (FM) ground state. While the rhombohedral structure leads to a magnetic frustration that prohibits such an arrangement, we have constructed a ferrimagnetic (FI) configuration that achieves the same basic purpose and is described in the inset of Table II for Ce_2Co_9Mg . In the mean-field local moment approximation, the Curie temperature can then be estimated as one third of this energy difference, measured on a per-Co basis. To quantify the effect of Mg on the Curie point, in addition to $CeCo_3$ and Ce_2MgCo_9 , we also study $CeMg_2Co_9$ (obtained by replacing a Ce by Mg in Ce_2MgCo_9). The resulting energy difference between the FI structure and FM structure is listed in Table II. In these calculations, we include spin-orbit coupling and a Hubbard U . For $CeCo_3$, we cannot stabilize any of the FI structures and the reported energy difference is simply between the FM and the nonmagnetic (NM) structure. This result may suggest some degree of itinerancy in the $CeCo_3$ -based magnetic materials.

As shown in Table II for $CeCo_3$, the NM state is 1.9 meV/Co above the FM ground state, resulting in a Curie temperature estimate of approximately 7 K. If we introduce one Mg at the Ce site (Ce_2MgCo_9), the energy difference between the FM and FI states is 54.8 meV/Co, which is nearly 27 times higher than the base compound $CeCo_3$.

Finally, if we add an additional Mg ($CeMg_2Co_9$), the difference between the FM and FI states is 87.8 meV/Co, which is 44 and 1.6 times higher than ΔE for $CeCo_3$ and Ce_2MgCo_9 , respectively. This analysis shows that upon Mg alloying in $CeCo_3$, the magnitude of the ΔE increases drastically. This result suggests that the mean-field J parameters should increase in $Ce_{3-x}Mg_xCo_9$ as x is increased, which would result in an enhanced Curie temperature. This result is in agreement with recent experimental results [25], which also find a manifold increase in the Curie temperature with Mg alloying. It is important to mention that, generally, mean-field theory is not immediately applicable to magnets with some degree of itinerant character. As these $CeCo_3$ -based magnets exhibit some degree of itinerancy, the actual theoretical values of the Curie point from a local moment approximation may be underestimated. Note that these results only provide an estimate of the ordering point and, for more accuracy, Monte Carlo calculations such as atomic spin dynamics [65–67] may be necessary.

IV. CONCLUSION

Motivated by a recent experimental study [25], we have carried out first-principles calculations to understand the remarkable transformation of paramagnetic $CeCo_3$ by Mg alloying into a material with magnetic properties (including large magnetization, Curie point, and magnetic anisotropy) comparable to those of a potential permanent magnet. We find this transformation to result from a combination of Stoner physics and the magnetic anisotropy of the Ce and Co atoms.

While the specific *physics* of this transformation is relatively particular to this compound, the general *behavior* exhibited here—the metamorphosis of an initially unpromising material into a potential permanent magnet via a simple alloying strategy—is, in fact, an underappreciated and powerful method for the production of permanent magnet materials. For example, the sister compound $NdCo_3$ [25,28] shows a large enhancement in its Curie point from 381 K for the base compound to 633 K for Nd_2MgCo_9 . Similarly, the low Curie point (216 K [68]) of Fe_2P , which has a favorably large magnetic anisotropy of 2.3 MJ/m³, increases to nearly 700 K via the simple substitution [69] of 40 at. % of phosphorus by silicon. Our own first-principles calculations [70] find that alloying of the low-Curie-point, low-magnetization ferrimagnet Fe_2Ta by hafnium yields a potential permanent magnet material with a magnetic anisotropy exceeding 2 MJ/m³.

The point of all these results is that there are likely *many* potential permanent magnet materials hidden in the guise of compounds that do not appear favorable for these applications, but that can, in fact, be made so by a simple alloying strategy. In fact, this approach, based on different

physics, has also been used to make thermoelectric materials, based on Si-Ge alloys, sufficiently useful to power the Voyager spacecraft, despite the unfavorably large thermal conductivity of both silicon and germanium. While such a strategy, applied to magnetic materials, may not ultimately yield a magnet as powerful as those based on $\text{Nd}_2\text{Fe}_{14}\text{B}$, it should produce a number of “gap magnets” [71], which may well fill in the substantial performance gap (measured as the energy product BH_{max}) between non-rare-earth magnets, such as alnico and ferrite, and the rare-earth magnets SmCo_5 and $\text{Nd}_2\text{Fe}_{14}\text{B}$. Such magnets will likely be of great utility to modern society considering the continuing worldwide industrialization and movement toward clean-energy technologies such as electric vehicles and wind turbines, which often use such magnets.

ACKNOWLEDGMENTS

This research was supported by the Critical Materials Institute, an Energy Innovation Hub funded by the U.S. Department of Energy, Office of Energy Efficiency and Renewable Energy, Advanced Manufacturing Office. This research used resources of the Compute and Data Environment for Science (CADES) at the Oak Ridge National Laboratory, which is supported by the Office of Science of the U.S. Department of Energy under Contract No. DE-AC05-00OR22725. The Department of Energy will provide public access to these results of federally sponsored research in accordance with the DOE Public Access Plan.

APPENDIX

1. Effect of lattice parameters and functional on magnetic properties of CeCo_3

The reported lattice parameters for CeCo_3 reported within the Inorganic Crystal Structure Database (ICSD) vary by about 4%. Hence, volume may play some role in determining the ground state of CeCo_3 . To check the volume dependence of magnetic properties for CeCo_3 , total energy and magnetic moments are computed as a function of the lattice constant within both LDA and GGA functionals. These results are shown in Fig. 7. Figure 7 shows that both LDA and GGA calculation find CeCo_3 to be close to a magnetic instability. While both LDA and GGA calculations favor a ferromagnetic state, at experimental lattice parameters within LDA, the energy difference between the ferromagnetic and nonmagnetic state ($E_{\text{FM}} - E_{\text{NM}}$) is only -1.9 meV on a per-Co basis. On the other hand, within GGA, this difference is about -21 meV per Co atom.

For CeCo_3 , the lattice parameters optimized within GGA ($a = 4.91$ Å, $c = 25.09$ Å) are in good agreement with the experimental lattice parameters, whereas LDA underestimates the lattice parameters ($a = 4.85$ Å, $c = 24.42$ Å). Figures 7(a) and 7(b) also show the behavior

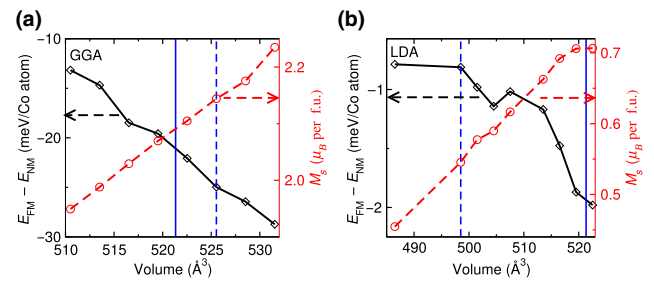


FIG. 7. The calculated energy difference between the FM and NM states on a per-Co basis (left y axis) and total unit-cell magnetic moment on a per-formula-unit basis as a function of unit-cell volume for CeCo_3 under (a) GGA and (b) LDA functionals. The optimized DFT volume (dashed lines) and experimental volume (solid lines) are also shown.

of the magnetic moments (plotted on the right y axis) in CeCo_3 as a function of volume. Both LDA and GGA curves show the expected increase in magnetic moments with increasing cell volume. One striking difference between the LDA and GGA functionals is the huge difference in calculated magnetization. At GGA optimized volume, the total spin moment in the unit cell is $2.1 \mu_B$ on a per-formula-unit basis, whereas with LDA a relatively smaller moment of $0.55 \mu_B$ on a per-formula-unit basis is observed. This result is in agreement with previous studies on weak itinerant magnets [38–41], where GGA is shown to overestimate the magnetic moments. Experimentally, CeCo_3 is often characterized as a Pauli paramagnetic [25,42], which is better captured in this case by the LDA functional. For $\text{Ce}_2\text{Co}_9\text{Mg}$, both the LDA and GGA functionals give consistent results. At experimental lattice parameters with a LDA functional, we find a total magnetic moment and MAE of $10.04 \mu_B$ and 0.48 MJ/m^3 , respectively. These values are in good agreement with the total magnetic moment and MAE of $10.9 \mu_B$ and MAE of 0.47 MJ/m^3 calculated within GGA. Again, all the calculations presented in the main text are done within LDA.

2. Determination of Stoner parameter (I)

The exchange splitting for CeCo_3 depends sensitively on the \mathbf{k} vector; therefore, here, we calculate the average exchange splitting (ΔE_{ex}), which can be defined as the difference of spin-up and spin-down eigenvalues in the corresponding bands [72,73]. This calculation gives us a value of about 0.185 eV. Now, the Stoner parameter can be calculated by using the relation $\Delta E_{\text{ex}} = I m_{\text{avg}}$ [46]. Here, m_{avg} is the average Co moment on a per-Co basis, which is about $0.33 \mu_B$ for CeCo_3 . This gives us I as 0.56 eV, which is very close to the value (0.49 eV) for elemental Co [47].

3. Convergence of MAE for $\text{Ce}_2\text{Co}_9\text{Mg}$

The convergence of the MAE with respect to the number of \mathbf{k} points for $\text{Ce}_2\text{Co}_9\text{Mg}$ is shown in Table III. The

TABLE III. Convergence of the MAE (in meV) with respect to the number of \mathbf{k} points in the full Brillouin zone.

No. of \mathbf{k} points	MAE (LDA+SOC)	MAE (LDA+SOC+ U)
300	2.91	2.86
1000	0.380	1.65
2000	0.484	2.16
4000	0.488	2.21
6000	0.473	2.13

MAE is calculated by subtracting the total energies along the in-plane $[1\bar{1}0]$ and out-of-plane $[111]$ direction. For comparison, both LDA+SOC and LDA+SOC+ U calculations are shown. A positive value of the MAE indicates uniaxial anisotropy. The MAE changes by less than 4% going from 4000 to 6000 \mathbf{k} points. All the calculations presented in the main text are done by using 4000 reducible \mathbf{k} points.

4. Valency of Ce

The nature of the Ce-4*f* valence state in Ce-transition metal complexes is still dubious. Several previous studies report the occurrence of mixed valency (Ce³⁺ and Ce⁴⁺) for the Ce ion [18,49–51,54]. The Ce valence can be further altered by doping [74], alloying [22,75], hydrogenation [76,77], etc. Our calculations find the valency of Ce in CeCo₃ to be dependent on the approximation used. For calculations without a U , as shown in the inset of Fig. 8, the localized Ce-4*f* states fall above the Fermi level (filled gray line), indicating tetravalency, while for the U value of 1.5 eV used here for Ce in CeCo₃, some of these states fall below E_F , indicating trivalency. Although this result does not confirm the occurrence of valence fluctuations in these compounds, the calculated magnetic properties seems to

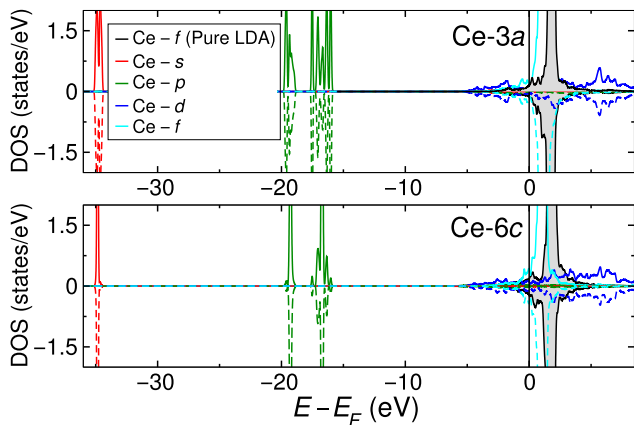


FIG. 8. DOS for nonequivalent Ce sites in CeCo₃ calculated under LDA+SOC+ U with $U = 1.5$ eV at the Ce site. DOS calculated within pure LDA (without SOC and without U) is shown with black (gray filled) lines.

suggest the possibility of mixed valency. For instance, the MAE of Ce₂Co₉Mg by considering Ce-*f* valence electrons as core states is very small (0.22 MJ/m³), suggesting that Ce-*f* valence electrons are important for magnetic properties. Therefore, within our study the Ce-*f* states are included as valence states and calculated magnetic properties are in good agreement with experiments.

- [1] D. C. Mattis and D. B. Butrymowicz, The theory of magnetism, *Phys. Today* **18**, 66 (1965).
- [2] J. M. Coey, *Magnetism and Magnetic Materials* (Cambridge University Press, Cambridge, UK, 2010).
- [3] C. G. Shull, W. Strauser, and E. Wollan, Neutron diffraction by paramagnetic and antiferromagnetic substances, *Phys. Rev.* **83**, 333 (1951).
- [4] S. W. Lovesey, *Theory of Neutron Scattering from Condensed Matter* (Clarendon Press, Oxford, UK, 1984).
- [5] C. G. Shull, Early development of neutron scattering, *Rev. Mod. Phys.* **67**, 753 (1995).
- [6] A. F. May, Y. Liu, S. Calder, D. S. Parker, T. Pandey, E. Cakmak, H. Cao, J. Yan, and M. A. McGuire, Magnetic order and interactions in ferrimagnetic Mn₃Si₂Te₆, *Phys. Rev. B* **95**, 174440 (2017).
- [7] A. F. May, S. Calder, D. S. Parker, B. C. Sales, and M. A. McGuire, Competing magnetic ground states and their coupling to the crystal lattice in CuFe₂Ge₂, *Sci. Rep.* **6**, 35325 (2016).
- [8] P. Hohenberg and W. Kohn, Inhomogeneous electron gas, *Phys. Rev.* **136**, B864 (1964).
- [9] W. Kohn and L. J. Sham, Self-consistent equations including exchange and correlation effects, *Phys. Rev.* **140**, A1133 (1965).
- [10] W. Kohn, Electronic structure of matter-wave functions and density functionals, *Rev. Mod. Phys.* **71**, 1253 (1999).
- [11] W. Kohn, A. D. Becke, and R. G. Parr, Density functional theory of electronic structure, *J. Phys. Chem.* **100**, 12974 (1996).
- [12] J. P. Perdew, J. A. Chevary, S. H. Vosko, K. A. Jackson, M. R. Pederson, D. J. Singh, and C. Fiolhais, Atoms, molecules, solids, and surfaces: Applications of the generalized gradient approximation for exchange and correlation, *Phys. Rev. B* **46**, 6671 (1992).
- [13] J. P. Perdew, A. Ruzsinszky, J. Tao, V. N. Staroverov, G. E. Scuseria, and G. I. Csonka, Prescription for the design and selection of density functional approximations: More constraint satisfaction with fewer fits, *J. Chem. Phys.* **123**, 062201 (2005).
- [14] J. P. Perdew, K. Burke, and M. Ernzerhof, Generalized Gradient Approximation Made Simple, *Phys. Rev. Lett.* **77**, 3865 (1996).
- [15] G. Kresse and J. Furthmüller, Efficient iterative schemes for ab initio total-energy calculations using a plane-wave basis set, *Phys. Rev. B* **54**, 11169 (1996).
- [16] D. J. Singh and L. Nordstrom, *Planewaves, Pseudopotentials, and the LAPW Method*, 2nd ed. (Springer, Berlin, 2006).
- [17] N. Drebov, A. Martinez-Limia, L. Kunz, A. Gola, T. Shigematsu, T. Eckl, P. Gumbusch, and C. Elsässer, Ab

- initio screening methodology applied to the search for new permanent magnetic materials, *New J. Phys.* **15**, 125023 (2013).
- [18] W. Körner, G. Krugel, and C. Elsässer, Theoretical screening of intermetallic ThMn₁₂-type phases for new hard-magnetic compounds with low rare earth content, *Sci. Rep.* **6**, 24686 (2016).
- [19] S. Sanvito, C. Oses, J. Xue, A. Tiwari, M. Zic, T. Archer, P. Tozman, M. Venkatesan, M. Coey, and S. Curtarolo, Accelerated discovery of new magnets in the Heusler alloy family, *Sci. Adv.* **3**, e1602241 (2017).
- [20] S. Curtarolo, W. Setyawan, S. Wang, J. Xue, K. Yang, R. H. Taylor, L. J. Nelson, G. L. Hart, S. Sanvito, M. Buongiorno-Nardelli, *et al.*, Aflowlib.org: A distributed materials properties repository from high-throughput ab initio calculations, *Comput. Mater. Sci.* **58**, 227 (2012).
- [21] J. Coey, Intrinsic magnetic properties of compounds with the Nd₂Fe₁₄B structure, *J. Less Common Met.* **126**, 21 (1986).
- [22] M. A. Susner, B. S. Conner, B. I. Saparov, M. A. McGuire, E. J. Crumlin, G. M. Veith, H. Cao, K. V. Shanavas, D. S. Parker, B. C. Chakoumakos, *et al.*, 2 flux growth and characterization of Ce-substituted Nd₂Fe₁₄B single crystals, *J. Magn. Magn. Mater.* **434**, 1 (2017).
- [23] Y. Tatetsu, S. Tsuneyuki, and Y. Gohda, First-principles Study of the Role of Cu in Improving the Coercivity of Nd-Fe-B Permanent Magnets, *Phys. Rev. Appl.* **6**, 064029 (2016).
- [24] M. Yi, H. Zhang, O. Gutfleisch, and B.-X. Xu, Multi-scale Examination of Strain Effects in Nd-Fe-B Permanent Magnets, *Phys. Rev. Appl.* **8**, 014011 (2017).
- [25] T. N. Lamichhane, V. Taufour, A. Palasyuk, Q. Lin, S. L. Bud'ko, and P. C. Canfield, Ce_{3-x}Mg_xCo₉: Transformation of a Pauli Paramagnet into a Strong Permanent Magnet, *Phys. Rev. Appl.* **9**, 024023 (2018).
- [26] P. Heller, Experimental investigations of critical phenomena, *Rep. Prog. Phys.* **30**, 731 (1967).
- [27] F. Keffer, *Handbuch der Physik* (Springer-Verlag, Berlin, 1966), Vol. 18-2.
- [28] V. Shtender, R. Denys, V. Paul-Boncour, I. Y. Zavaliiy, Y. V. Verbovytsky, and D. Taylor, Crystal structure, hydrogen absorption-desorption behavior and magnetic properties of the Nd_{3-x}Mg_xCo₉ alloys, *J. Alloys Compd.* **695**, 1426 (2017).
- [29] *WIEN2K, An Augmented Plane Wave + Local Orbitals Program for Calculating Crystal Properties.*
- [30] M. Brooks, L. Nordstrom, and B. Johansson, Origin and ab initio evaluation of magnetic interactions in rare earth intermetallics, *J. Phys. Condens. Matter* **3**, 3393 (1991).
- [31] P. Larson, I. Mazin, and D. Papaconstantopoulos, Calculation of magnetic anisotropy energy in SmCo₅, *Phys. Rev. B* **67**, 214405 (2003).
- [32] P. Larson and I. Mazin, Calculation of magnetic anisotropy energy in YCo₅, *J. Magn. Magn. Mater.* **264**, 7 (2003).
- [33] V. I. Anisimov, I. Solovyev, M. Korotin, M. Czyżyk, and G. Sawatzky, Density-functional theory and NiO photoemission spectra, *Phys. Rev. B* **48**, 16929 (1993).
- [34] A. Liechtenstein, V. Anisimov, and J. Zaanen, Density-functional theory and strong interactions: Orbital ordering in Mott-Hubbard insulators, *Phys. Rev. B* **52**, R5467 (1995).
- [35] A. Shick, A. Liechtenstein, and W. Pickett, Implementation of the LDA+*U* method using the full-potential linearized augmented plane-wave basis, *Phys. Rev. B* **60**, 10763 (1999).
- [36] G. K. Madsen and P. Novák, Charge order in magnetite. An LDA+*U* study, *Europhys. Lett.* **69**, 777 (2005).
- [37] I. Mazin, D. Singh, and A. Aguayo, in *Physics of Spin in Solids: Materials, Methods and Applications* (Springer, Berlin, 2004), p. 139.
- [38] S. Khmelevskiy, P. Mohn, J. Redinger, and M. Weinert, Magnetism on the Surface of the Bulk Paramagnetic Intermetallic Compound YCo₂, *Phys. Rev. Lett.* **94**, 146403 (2005).
- [39] A. Aguayo, I. Mazin, and D. Singh, Why Ni₃Al is an Itinerant Ferromagnet but Ni₃Ga is Not, *Phys. Rev. Lett.* **92**, 147201 (2004).
- [40] P. Larson, I. Mazin, and D. Singh, Magnetism, critical fluctuations, and susceptibility renormalization in Pd, *Phys. Rev. B* **69**, 064429 (2004).
- [41] M. Sieberer, S. Khmelevskiy, and P. Mohn, Magnetic instability within the series TCu₃N (*T* = Pd, Rh and Ru): A first-principles study, *Phys. Rev. B* **74**, 014416 (2006).
- [42] K. Buschow, Magnetic properties of CeCo₃, Ce₂Co₇ and CeNi₃ and their ternary hydrides, *J. Less Common Met.* **72**, 257 (1980).
- [43] R. Lemaire, Magnetic properties of the intermetallic compounds of cobalt with the rare earth metals and yttrium, *Cobalt* **33**, 201 (1966).
- [44] The spin moment at Ce and Co site presented in Table I is the spin moment only within the Ce or Co sphere, and does not include the contribution from interstitial moment. The contribution from interstitial and orbital moment is included in the total magnetic moment.
- [45] E. C. Stoner, *et al.*, Collective electron ferromagnetism II. Energy and specific heat, *Proc. R. Soc. Lond. A* **169**, 339 (1939).
- [46] L. Ortenzi, S. Biermann, O. K. Andersen, I. Mazin, and L. Boeri, Competition between electron-phonon coupling and spin fluctuations in superconducting hole-doped CuBiSO, *Phys. Rev. B* **83**, 100505 (2011).
- [47] J. Janak, Uniform susceptibilities of metallic elements, *Phys. Rev. B* **16**, 255 (1977).
- [48] B. C. Sales, PhD dissertation, University of California, San Diego, 1974.
- [49] J. Coey, J. Allan, A. Minakov, and Y. V. Bugaslavsky, Ce₂Fe₁₇: Mixed valence or 4f band?, *J. Appl. Phys.* **73**, 5430 (1993).
- [50] T. Jarlborg, Role of thermal disorder for magnetism and the α - γ transition in cerium: Results from density-functional theory, *Phys. Rev. B* **89**, 184426 (2014).
- [51] A. Alam and D. D. Johnson, Mixed valency and site-preference chemistry for cerium and its compounds: A predictive density-functional theory study, *Phys. Rev. B* **89**, 235126 (2014).
- [52] M. Matsumoto, M. J. Han, J. Otsuki, and S. Y. Savrasov, First-principles Simulations of Heavy Fermion Cerium Compounds based on the Kondo Lattice, *Phys. Rev. Lett.* **103**, 096403 (2009).
- [53] B. Sales and R. Viswanathan, Demagnetization due to inter-configuration fluctuations in the RE-Cu₂Si₂ compounds, *J. Low Temp. Phys.* **23**, 449 (1976).

- [54] B. Sales and D. Wohlleben, Susceptibility of Interconfiguration-fluctuation Compounds, *Phys. Rev. Lett.* **35**, 1240 (1975).
- [55] B. C. Sales, A model for the thermodynamic properties of metallic rare earth systems with an unstable valence, *J. Low Temp. Phys.* **28**, 107 (1977).
- [56] T. Pandey, M.-H. Du, and D. S. Parker, Tuning the Magnetic Properties and Structural Stabilities of the 2-17-3 Magnets $\text{Sm}_2\text{Fe}_{17}\text{X}_3$ ($\text{X} = \text{C}, \text{N}$) by Substituting La or Ce for Sm, *Phys. Rev. Appl.* **9**, 034002 (2018).
- [57] T. Pandey and D. S. Parker, Magnetic properties and magnetocrystalline anisotropy of $\text{Nd}_2\text{Fe}_{17}$, $\text{Nd}_2\text{Fe}_{17}\text{X}_3$, and related compounds, *Sci. Rep.* **8**, 3601 (2018).
- [58] P. Larson and I. Mazin, Magnetic properties of SmCo_5 and YCo_5 , *J. Appl. Phys.* **93**, 6888 (2003).
- [59] J.-X. Zhu, M. Janoschek, R. Rosenberg, F. Ronning, J. Thompson, M. A. Torrez, E. D. Bauer, and C. D. Batista, LDA+DMFT Approach to Magnetocrystalline Anisotropy of Strong Magnets, *Phys. Rev. X* **4**, 021027 (2014).
- [60] G. Daalderop, P. Kelly, and M. Schuurmans, Magnetic anisotropy of a free-standing Co monolayer and of multilayers which contain Co monolayers, *Phys. Rev. B* **50**, 9989 (1994).
- [61] V. Antropov, L. Ke, and D. Berg, Constituents of magnetic anisotropy and a screening of spin-orbit coupling in solids, *Solid State Commun.* **194**, 35 (2014).
- [62] L. Ke and M. van Schilfgaarde, Band-filling effect on magnetic anisotropy using a Green's function method, *Phys. Rev. B* **92**, 014423 (2015).
- [63] L. Ke, D. Kukusta, and D. D. Johnson, Origin of magnetic anisotropy in doped $\text{Ce}_2\text{Co}_{17}$ alloys, *Phys. Rev. B* **94**, 144429 (2016).
- [64] P. Bruno, Tight-binding approach to the orbital magnetic moment and magnetocrystalline anisotropy of transition-metal monolayers, *Phys. Rev. B* **39**, 865 (1989).
- [65] B. Skubic, J. Hellsvik, L. Nordström, and O. Eriksson, A method for atomistic spin dynamics simulations: Implementation and examples, *J. Phys. Condens. Matter* **20**, 315203 (2008).
- [66] R. F. Evans, W. J. Fan, P. Chureemart, T. A. Ostler, M. O. Ellis, and R. W. Chantrell, Atomistic spin model simulations of magnetic nanomaterials, *J. Phys. Condens. Matter* **26**, 103202 (2014).
- [67] O. Eriksson, A. Bergman, L. Bergqvist, and J. Hellsvik, *Atomistic Spin Dynamics: Foundations and Applications* (Oxford University Press, Oxford, UK, 2017).
- [68] P. Jernberg, A. Yousif, L. Häggström, and Y. Andersson, A Mössbauer study of $\text{Fe}_2\text{P}_{1-x}\text{Si}_x$ ($x \leq 0.35$), *J. Solid State Chem.* **53**, 313 (1984).
- [69] E. K. Delczeg-Czirjak, L. Delczeg, M. P. J. Punkkinen, B. Johansson, O. Eriksson, and L. Vitos, Ab initio study of structural and magnetic properties of Si-doped Fe_2P , *Phys. Rev. B* **82**, 085103 (2010).
- [70] T. Pandey and D. S. Parker, Magnetic properties of Fe_2Ta under hafnium doping, In preparation.
- [71] J. Coey, Permanent magnets: Plugging the gap, *Scr. Mater.* **67**, 524 (2012).
- [72] J. Kübler, *Theory of Itinerant Electron Magnetism* (Oxford University Press, Oxford, UK, 2017), Vol. 106.
- [73] H. L. Zhuang, P. Kent, and R. G. Hennig, Strong anisotropy and magnetostriction in the two-dimensional stoner ferromagnet Fe_3GeTe_2 , *Phys. Rev. B* **93**, 134407 (2016).
- [74] J. Jin, Y. Zhang, G. Bai, Z. Qian, C. Wu, T. Ma, B. Shen, and M. Yan, Manipulating Ce valence in $\text{RE}_2\text{Fe}_{14}\text{B}$ tetragonal compounds by La-Ce co-doping: Resultant crystallographic and magnetic anomaly, *Sci. Rep.* **6**, 30194 (2016).
- [75] A. Alam, M. Khan, R. W. McCallum, and D. D. Johnson, Site-preference and valency for rare-earth sites in $(\text{R-Ce})_2\text{Fe}_{14}\text{B}$ magnets, *Appl. Phys. Lett.* **102**, 042402 (2013).
- [76] O. Isnard, S. Miraglia, M. Guillot, and D. Fruchart, Hydrogen effects on the magnetic properties of RFe_{11}Ti compounds, *J. Alloys Compd.* **275**, 637 (1998).
- [77] J. Chaboy, A. Marcelli, L. Bozukov, F. Baudelet, E. Dartyge, A. Fontaine, and S. Pizzini, Effect of hydrogen absorption on the cerium electronic state in $\text{CeFe}_{11}\text{Ti}$: An x-ray-absorption and circular-magnetic-dichroism investigation, *Phys. Rev. B* **51**, 9005 (1995).